Turkish Journal of Chemistry

Volume 38 | Number 6 Article 8

1-1-2014

Coupling ferrocene to brominated tetraazaporphyrin: exploring an alternative synthetic pathway for preparation of ferrocene-containing tetraazaporphyrins

VICTOR N. NEMYKIN

ELENA A. MAKAROVA

NATHAN R. ERICKSON

PAVLO V. SOLNTSEV

TÜBİTAK

Turkish Journal of Chemistry

http://journals.tubitak.gov.tr/chem/

Research Article

Turk J Chem
(2014) 38: 1027 – 1045

doi:10.3906/kim-1406-19

Coupling ferrocene to brominated tetraazaporphyrin: exploring an alternative synthetic pathway for preparation of ferrocene-containing tetraazaporphyrins

Victor N. NEMYKIN[1,*], **Elena A. MAKAROVA**[1,2], **Nathan R. ERICKSON**[1], **Pavlo V. SOLNTSEV**[1]

[1]Department of Chemistry & Biochemistry, University of Minnesota Duluth, Duluth, MN, USA
[2]Organic Intermediates and Dyes Institute, Moscow, Russia

Received: 10.06.2014 • **Accepted:** 01.08.2014 • **Published Online:** 24.11.2014 • **Printed:** 22.12.2014

Abstract: A Castro–Stephens coupling reaction between metal-free 3(2),8(7)-dibromo- 2(3),7(8),12(13),17(18)-tetra-*tert*-butyl-5,10,15,20-tetraazaporphyrin and (ferrocenylethynyl)copper resulted in the formation of copper 2(3),7(8),12(13),17(18)-tetra-*tert*-butyl-3(2),8(7)-di(ferrocenylethynyl)-5,10,15,20-tetraazaporphyrin and copper 2(3),7(8),12(13),17(18)-tetra-*tert*-butyl-3(2)-ferrocenylethynyl-5,10,15,20-tetraazaporphyrin, which were separated in the form of 2 positional isomers along with copper 3(2)-bromo-2(3),7(8),12(13),17(18)-tetra-*tert*-butyl-5,10,15,20-tetraazaporphyrin and copper 2(3),7(8),12(13),17(18)-tetra-*tert*-butyl-5,10,15,20-tetraazaporphyrin. A similar reaction with metal-free 3(2),8(7),13(12),18(17)-tetrabromo-2(3),7(8),12(13),17(18)-tetra-*tert*-butyl-5,10,15,20-tetraazaporphyrin resulted in only a trace amount of 3(2),8(7),13(12)-tribromo-2(3),7(8),12(13),17(18)-tetra-*tert*-butyl-18(17)-ferrocenylethynyl-5,10,15,20-tetraazaporphyrin, while no products with larger number of organometallic substituents were observed. Direct coupling between ferrocenelithium and 3(2),8(7)-dibromo-2(3),7(8),12(13),17(18)-tetra-*tert*-butyl-5,10,15,20-tetraazaporphyrin resulted in a debromination reaction accompanied by very minor dimerization of the tetraazaporphyrin core, which was explained based on the steric properties of the parent tetraazaporphyrin. The target compounds were characterized using APCI mass spectrometry, UV-vis, and MCD spectroscopy, while the electronic structure of ferrocenylethyl-containing products was predicted by DFT approach. X-ray structures of individual positional isomers of copper 2-bromo-3,7,12,18-tetra-*tert*-butyl-5,10,15,20-tetraazaporphyrin and 3, 7, 12,18-tetrabromo-2,8,13,17-tetra-*tert*-butyl-5,10,15,20-tetraazaporphyrin were also discussed.

Key words: Ferrocene, tetraazaporphyrin, coupling reaction, magnetic circular dichroism, UV-vis spectra, density functional theory

1. Introduction

Phthalocyanines and their analogues[1–4] are well-established platforms for modern high-tech applications, which include but are not limited to photodynamic therapy of cancer,[5,6] catalysis,[7–9] optical recording,[10] light-harvesting,[11] molecular electronics,[12] and sensors.[13] Ferrocene is a well-known electron-donating substituent that can be used in numerous prospective donor–acceptor dyads for light-harvesting and molecular switches.[14] In addition, such systems were suggested as potentially useful components for redox-driven fluorescence, molecular electronics, ion-recognition, and optical limiting devices.[15] Ferrocene-containing aromatic macrocycles and their analogues with direct, alkenyl, or alkynyl ferrocene-to-π-system conjugation motifs were suggested

*Correspondence: vnemykin@d.umn.edu

as prospective platforms for several applications because of their rich redox chemistry and redox-switchable spectroscopic versatility.[16–18] Electron-transfer processes in numerous ferrocene-containing porphyrins with such conjugated bridges have been intensively investigated over the last decade.[19–35] Reports on conjugated porphyrin analogues such as phthalocyanines,[36,37] corroles,[38,39] and (aza)BODIPYs,[40–44] however, are quite rare. Finally, there are only 2 brief reports, published by us, on ferrocene-containing tetraazaporphyrins with conjugated into π-system ferrocene substituents.[45,46] Both known tetraazaporphyrins with direct ferrocene–macrocycle bonds were prepared from dicyanoferroceneethylene[47] and tricyanovinylferrocene[48] precursors and have mild solubility in low-polarity solvents, which is critical for an accurate evaluation of their electron-transfer properties. It is well known that introduction of *tert*-butyl groups into phthalocyanines and tetraazaporphyrins results in dramatic increases in their solubility in nonpolar solvents and significant decreases in aggregation ability.[1–3] Functionalization of tetra-*tert*-butyltetraazaporphyrins with ferrocene groups, however, has never been targeted. Thus, in this paper, we report the first attempts on such functionalization with ferrocene lithium and (ferrocenylethynyl)copper as ferrocene group precursors (Schemes 1–3).

2. Results and discussion

2.1. Synthesis and characterization of ferrocene-containing tetraazaporphyrins

Because we were interested in evaluation of the long-range electronic coupling between multiple ferrocene substituents in tetraazaporphyrins, 3(2),7(8)-dibromo-2(3),7(8),12(13),17(18)-tetra-*tert*-butyl-5,10,15,20-tetraazaporphyrin (**1**) and 3(2),8(7),13(12),18(17)-tetrabromo-2(3),7(8),12(13),17(18)-tetra-*tert*-butyl-5,10,15,20-tetraazaporphyrin (**2**) were used in coupling reactions (Schemes 1–3). Both precursors were prepared using a previously reported bromination reaction.[49] In the case of the reaction between dibromotetraazaporphyrin **1** and excess of ferrocene lithium (with or without presence of palladium salt), 2 groups of products were detected by mass spectrometry after filtering of the reaction mixture over a small portion of silica gel. The first group of products (first fraction from short column separation, 3 individual compounds, Figure 1) consists of trace amounts of the tetraazaporphyrin dimers **3**–**5** (Scheme 1), which could be viewed as a Wurtz–Fittig-type reaction products.[50] The second type of this coupling reaction product (second and third fractions from short column separation, 2 products each fraction) comprises monobromotetraazaporphyrin **6**, standard tetra-*tert*-butyltetraazaporphyrin **7**, and starting dibromo- compound **1**. The presence of compounds **6** and **7** clearly suggests the stepwise elimination of bromine atoms from the starting material **1**. All our attempts to identify the ferrocene-containing tetraazaporphyrins in the reaction mixture were unsuccessful. In order to explain the low reactivity of the ferrocenyllithium in the coupling reaction with dibromo compound **1**, we conducted DFT calculations and found that bulky *tert*-butyl groups in **1** create large steric strain for the coupling reaction for formation of a direct ferrocene–tetraazaporphyrin bond.

In order to reduce steric interactions between the *tert*-butyl groups in tetraazaporphyrin and ferrocene substituents, we tested the Castro–Stephens coupling reaction[51] between dibromo tetraazaporphyrin **1** and (ferrocenylethynyl)copper as ferrocene group precursor (Scheme 2). After elimination of the insoluble and polar impurities by filtration over a small amount of silica gel with chloroform, a blue-violet fraction, which contains all tetraazaporphyrins, was purified using size exclusion chromatography followed by preparative thin-layer chromatography applied to each fraction obtained from the size exclusion column. Copper tetraazaporphyrins **8**–**11** were separated by the size exclusion method (Scheme 2). Positional isomers of complexes **8**–**10** were further separated using TLC approach (see Experimental section for details). Since a large excess of (ferro-

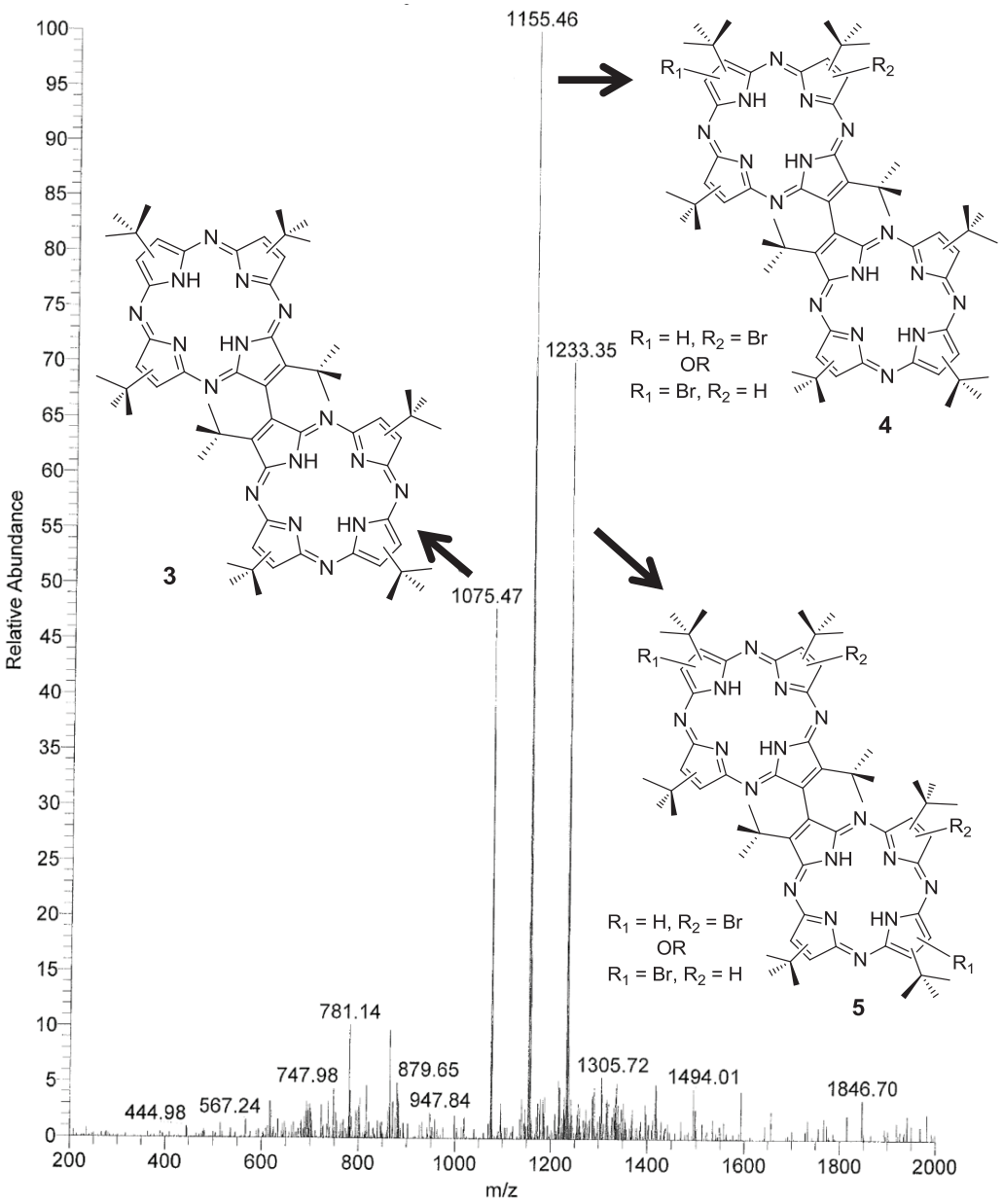

Figure 1. APCI MS spectrum of tetraazaporphyrin dimers **3**–**5**.

cenylethynyl)copper was used in the reaction, it is not surprising that all reaction products undergo metal insertion into the macrocyclic core. Similar to the reaction presented in Scheme 1, the formation of mono-bromo complex **10** and copper tetra-*tert*-butyltetraazaporphyrin **11** is indicative of the bromine elimination process during the coupling reaction. The presence of di- and monoferrocene-containing complexes **8** and **9** is clearly suggestive of the possibility of ferrocene group insertion into a highly sterically crowded tetra-*tert*-butyltetraazaporphyrin core. Although the overall yield of all positional isomers of mono-ferrocenyl-containing complex **9** is reasonable (22.4%), the reaction yield of the target diferrocenyl complex **8** (1.4% for all positional isomers) is rather disappointing. All our attempts to increase the yield of the diferrocenyl complex **8** under Castro–Stephens coupling reaction conditions were unsuccessful.

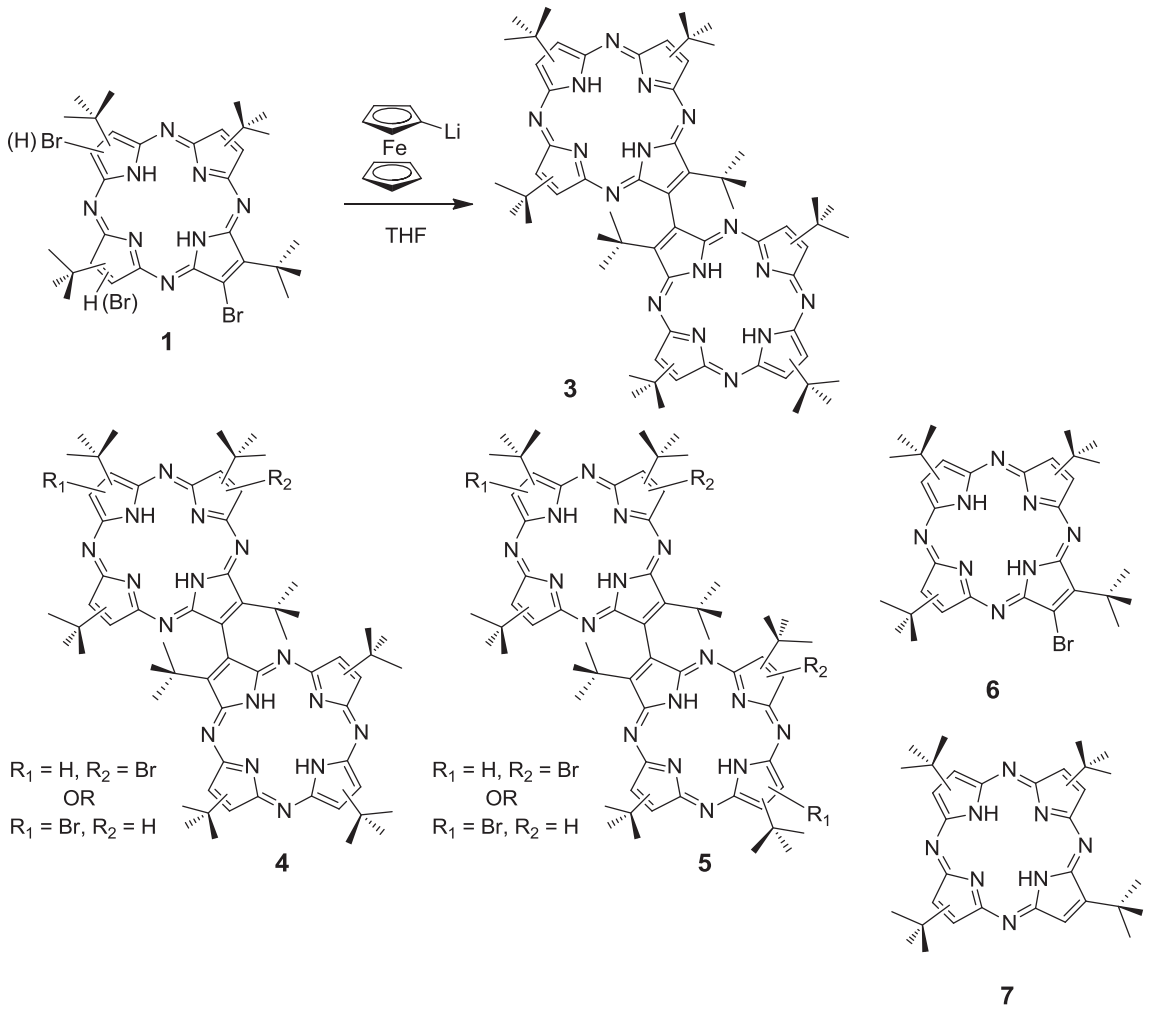

Scheme 1. Products identified by APCI MS approach for the reaction between tetraazaporphyrin **1** and ferrocenyl lithium.

Separated by the size exclusion chromatography diferrocenyl complex **8** can be further separated into 2 positional isomers by the TLC approach. These 2 positional isomers (**8a** and **8b**) have very close R_f values and the same molecular ion and isotope pattern, as well as indistinguishable UV-vis and MCD spectra. In theory, diferrocenyl complex **8** can be a mixture of *cis*- or *trans*-positional isomers (Figure 2). Since UV-vis and MCD spectra of complexes **8a** and **8b** are indistinguishable, they should belong either to *cis*- or *trans*-isomers but not both. In order to clarify the nature of **8a** and **8b** we investigated collision induced dissociation of the molecular ion in an APCI probe (Figures 3 and 4). As can be clearly seen, only ferrocene, methyl, and *tert*-butyl groups can be fragmented from the parent ion, while the tetraazaporphyrin core remains intact. Because the macrocyclic core is unchanged up to 90% of the collision energy, it is impossible to assign complexes **8a** and **8b** to *cis*- or *trans*-form. In the case of mono-ferrocenyl-containing complex **9** the TLC method allowed the separation of 3 positional isomers, **9a**–**9c**, which again have indistinguishable UV-vis and MCD spectra as well as the same molecular ion peak (Figure 5). In this case, positional isomers are defined by the relative positions of the *tert*-butyl groups in the macrocyclic core (Figure 6).

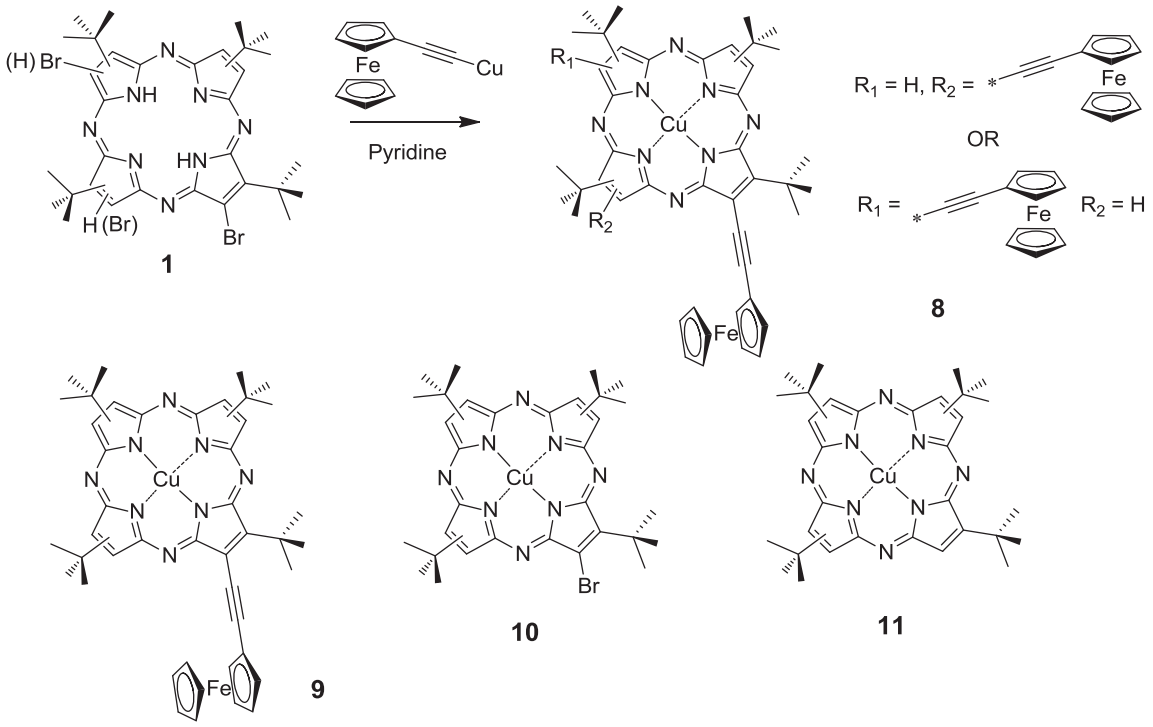

Scheme 2. Products identified by APCI MS approach for the reaction between tetraazaporphyrin **1** and (ferrocenylethynyl)copper.

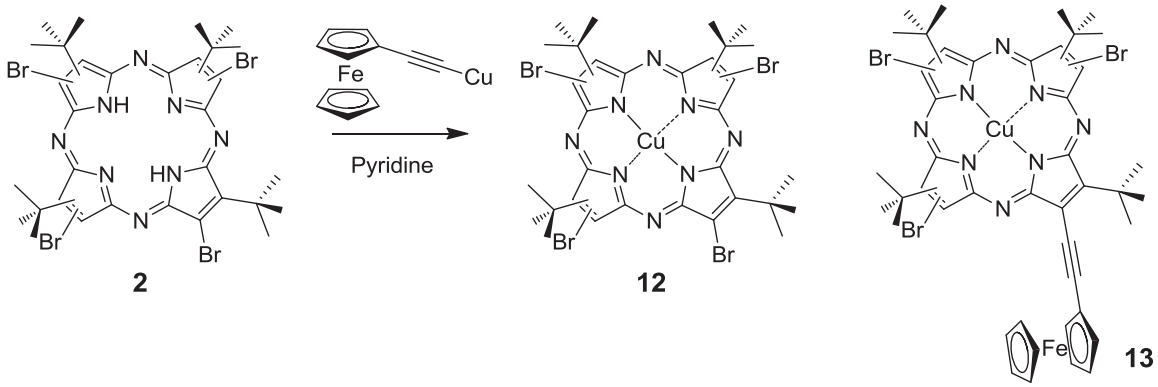

Scheme 3. Products identified by APCI MS approach for the reaction between tetraazaporphyrin **2** and (ferrocenylethynyl)copper.

In order to avoid the *cis*- and *trans*-positional isomers dilemma in complex **8**, we also tested the Castro–Stephens coupling reaction[51] between tetrabromo tetraazaporphyrin **2** and (ferrocenylethynyl)copper as ferrocene group precursor (Scheme 3). APCI analysis of the reaction mixture revealed the presence of the copper tetrabromo tetraazaporphyrin **12** and copper mono-ferrocenyl-containing tribromo tetraazaporphyrin **13**. The latter complex was only separated in trace amounts and was not further characterized. The low reactivity of compound **2** in the coupling reaction can be explained on the basis of the electron-withdrawing character of bromine atoms.

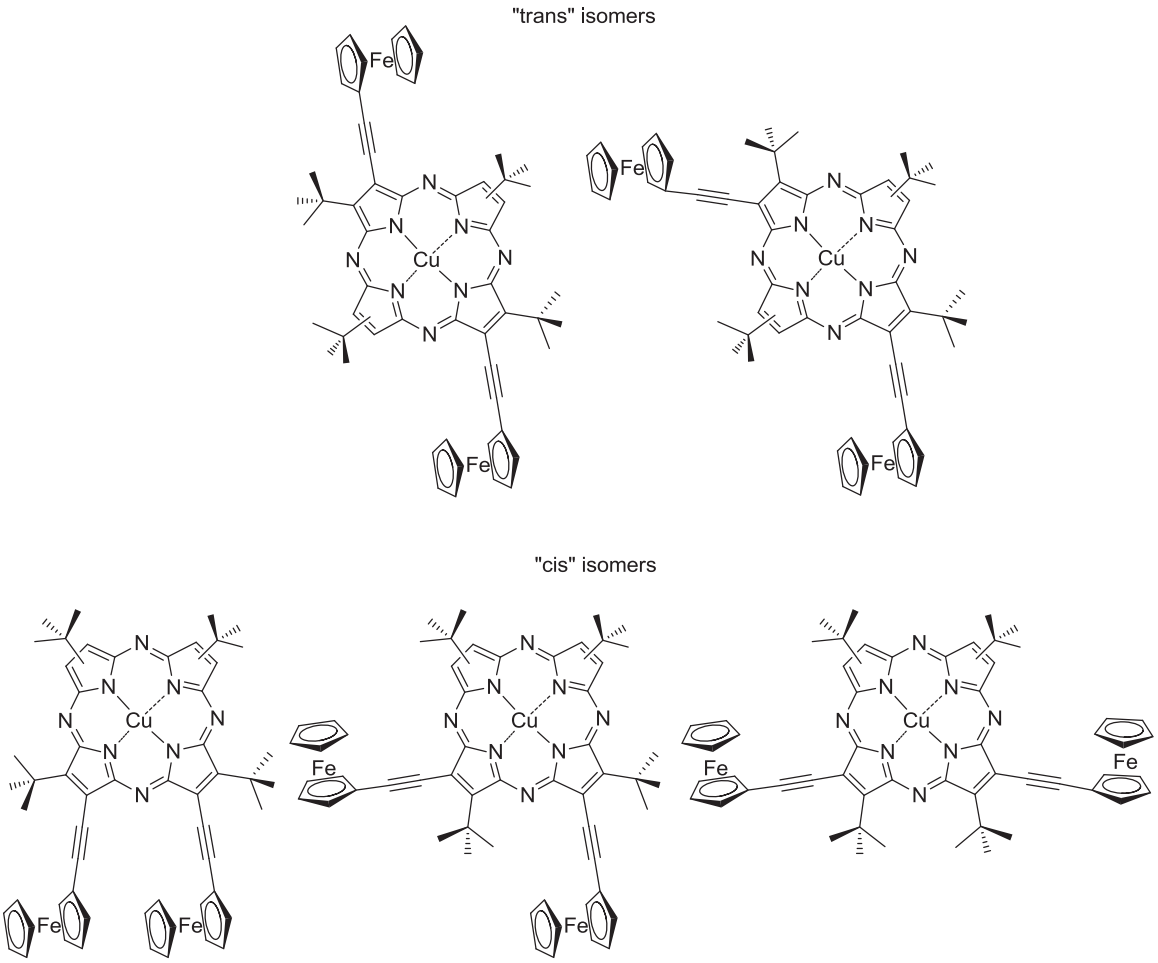

Figure 2. Ferrocenylethyl-based possible positional isomers of complex **8**.

2.2. Optical properties and electronic structures of ferrocene-containing tetraazaporphyrins

UV-vis and MCD spectra of mono- and diferrocenyl-containing complexes **9a** and **8a** are shown in Figures 7 and 8. In general, UV-vis spectra of these compounds are dominated by absorption in Q- ($\sim$600 nm) and B-band ($\sim$350 nm) regions. Upon stepwise addition of the ferrocenylethynyl substituents to the tetraazaporphyrin core, the Q-band undergoes a low-energy shift and becomes significantly broader compared to the Q-band in the parent halogenated tetraazaporphyrins (Figure 9). Indeed, the Q-band in the mono-ferrocenyl derivative shifted to 593 nm and the Q-band in the bis-ferrocene complex was observed at 602 nm (Figures 7 and 8). Similarly, MCD spectra of **9a** and **8a** are dominated by the MCD Faraday pseudo A-terms in Q- and B-regions centered at 592 and 340 nm in mono-ferrocenyl complex **9** and 599 and 344 nm in bis-ferrocenyl complex **8**, respectively. Q-band profiles in complexes **8** and **9** as observed in their UV-vis and MCD spectra are clearly indicative of the presence of multiple overlapping bands in this spectral region.

In order to explain the significant broadening of the Q-band region in ferrocenyl-containing complexes **8** and **9**, we conducted DFT calculations on the closed shell zinc analogues of **8** and **9** (**8Zn** and **9Zn**). We used closed shell zinc ion in calculations in order to clarify the electronic structure features, accelerate calculations, and to accommodate the minor influence of the copper ion on the UV-vis and MCD spectra of complexes **8** and **9**. In the case of bis-ferrocenyl-containing complex **8**, both *cis*- and *trans*-geometries were considered (these

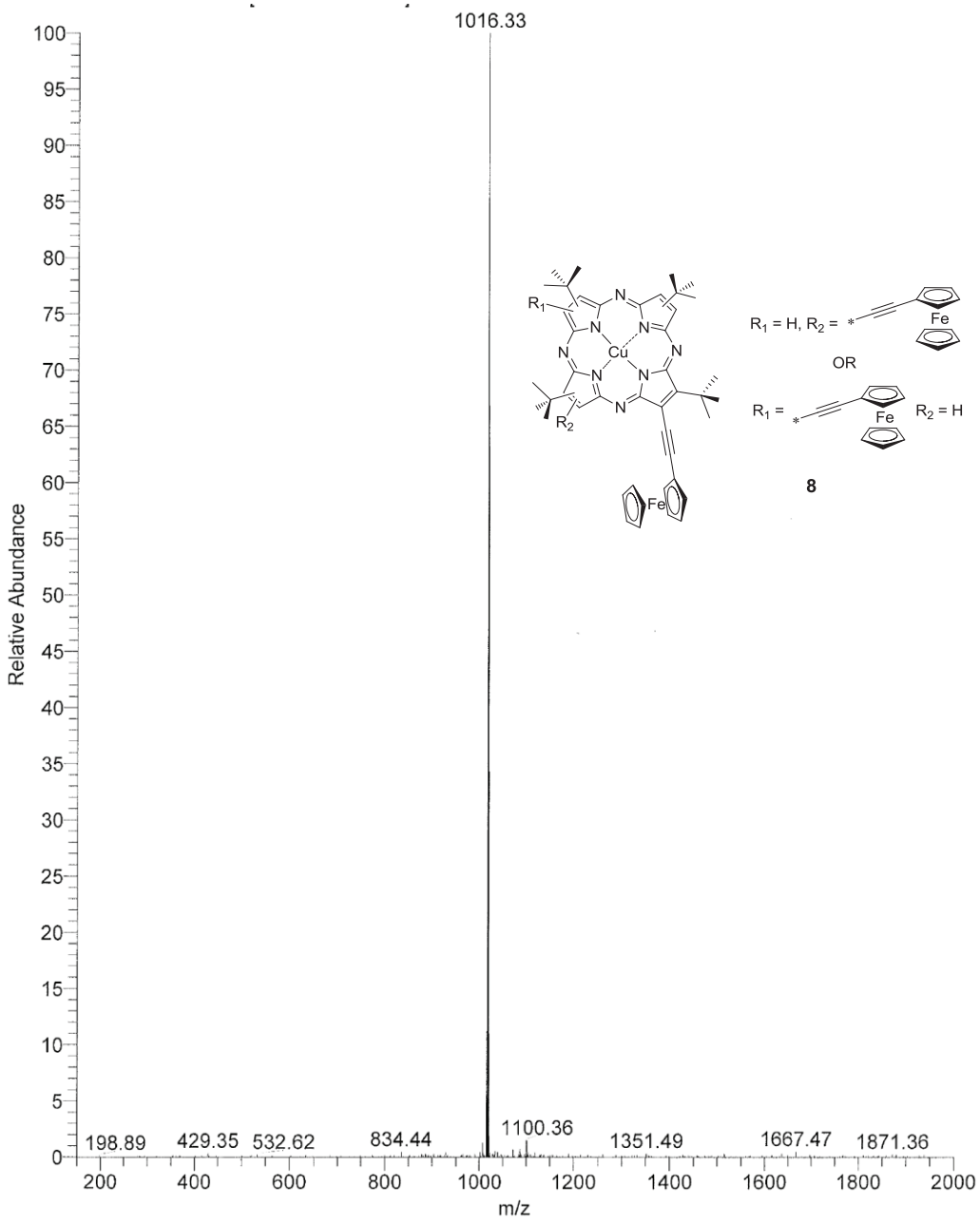

Figure 3. APCI MS spectrum of complex **8**.

are labeled as **cis8Zn** and **trans8Zn**, respectively). Because of the minor influence of the *tert*-butyl groups on the electronic structure of the target compounds, they were omitted from calculations. The molecular orbital energy diagram, molecular orbital compositions, and representative shapes of important molecular orbitals predicted using the TPSSh exchange-correlation functional (10% of Hartree–Fock exchange) and LANL2DZ basis set are shown in Figures 10–14. The electronic structures of ferrocene-containing tetraazaporphyrins have many similarities with earlier reported electronic structures of the ferrocene-containing porphyrins.[23−26] In particular, predominantly ferrocene-centered MOs have higher energies compared to the tetraazaporphyrin-centered occupied π-orbitals. In all cases, the HOMO is an almost pure ferrocene-centered orbital with

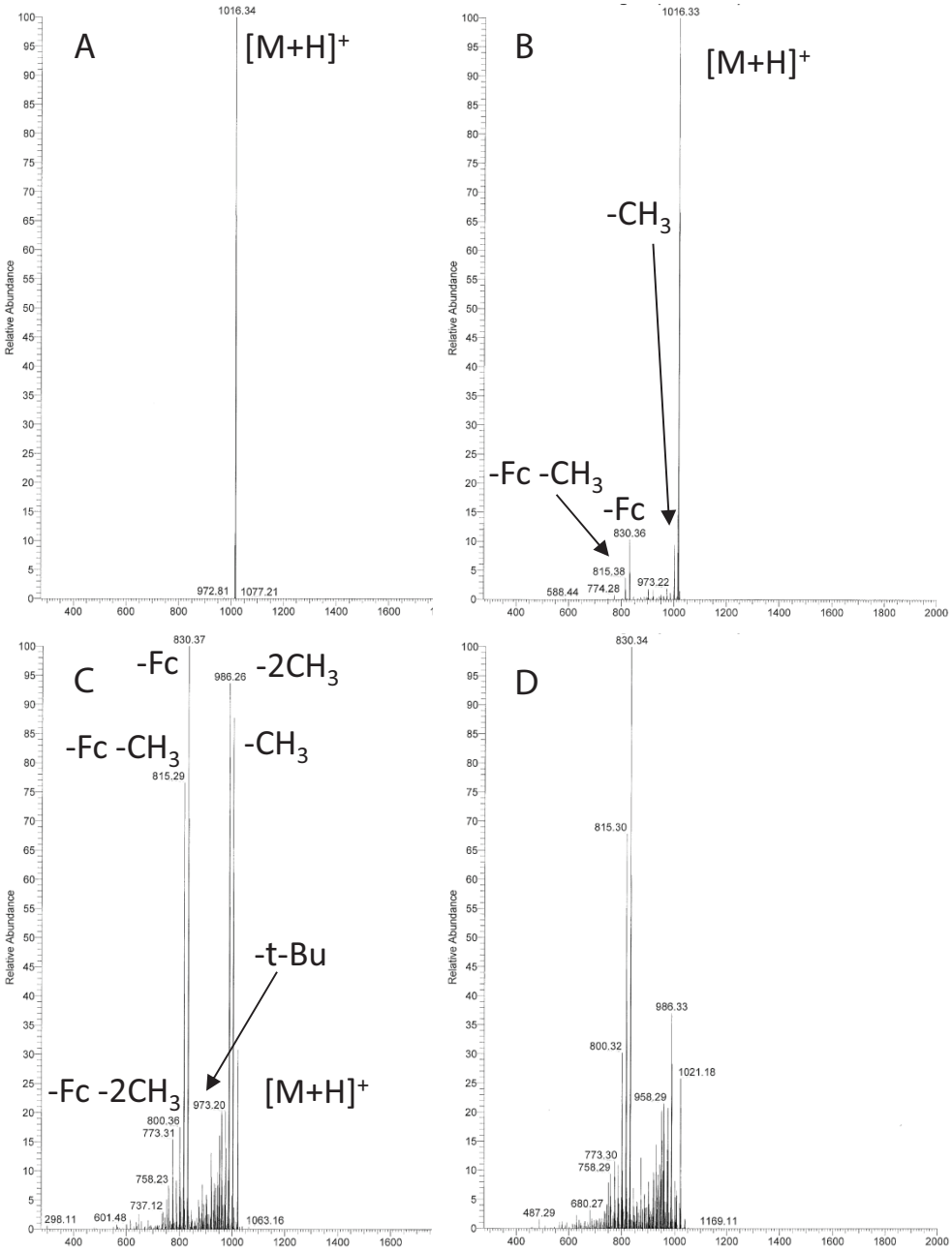

Figure 4. APCI MS/MS spectra of complex **8** at 15% (A), 30% (B), 45% (C), and 60% (D) CID energies.

significant contribution from the –C≡C– fragment. In the case of mono-derivative **9Zn**, Gouterman's "a_{1u}"-type tetraazaporphyrin orbital is delocalized over HOMO-2 to HOMO-4 MOs and heavily mixed with ferrocene-centered electron densities. In the case of bis-derivatives **cis8Zn** and **trans8Zn**, Gouterman's "a_{1u}"-type tetraazaporphyrin orbital contributes significantly to HOMO-4 and HOMO-8 (**cis8Zn**) and HOMO-4 and HOMO-7 (**trans8Zn**). Gouterman's "a_{2u}"-type (with most electron density located at the *meso*- and pyrrolic nitrogen atoms) tetraazaporphyrin-centered π-orbital has lower energy than the "a_{1u}"-type π-orbital. The LUMO and LUMO+1 are predominantly tetraazaporphyrin-centered π^* orbitals that resemble Gouterman's[52]

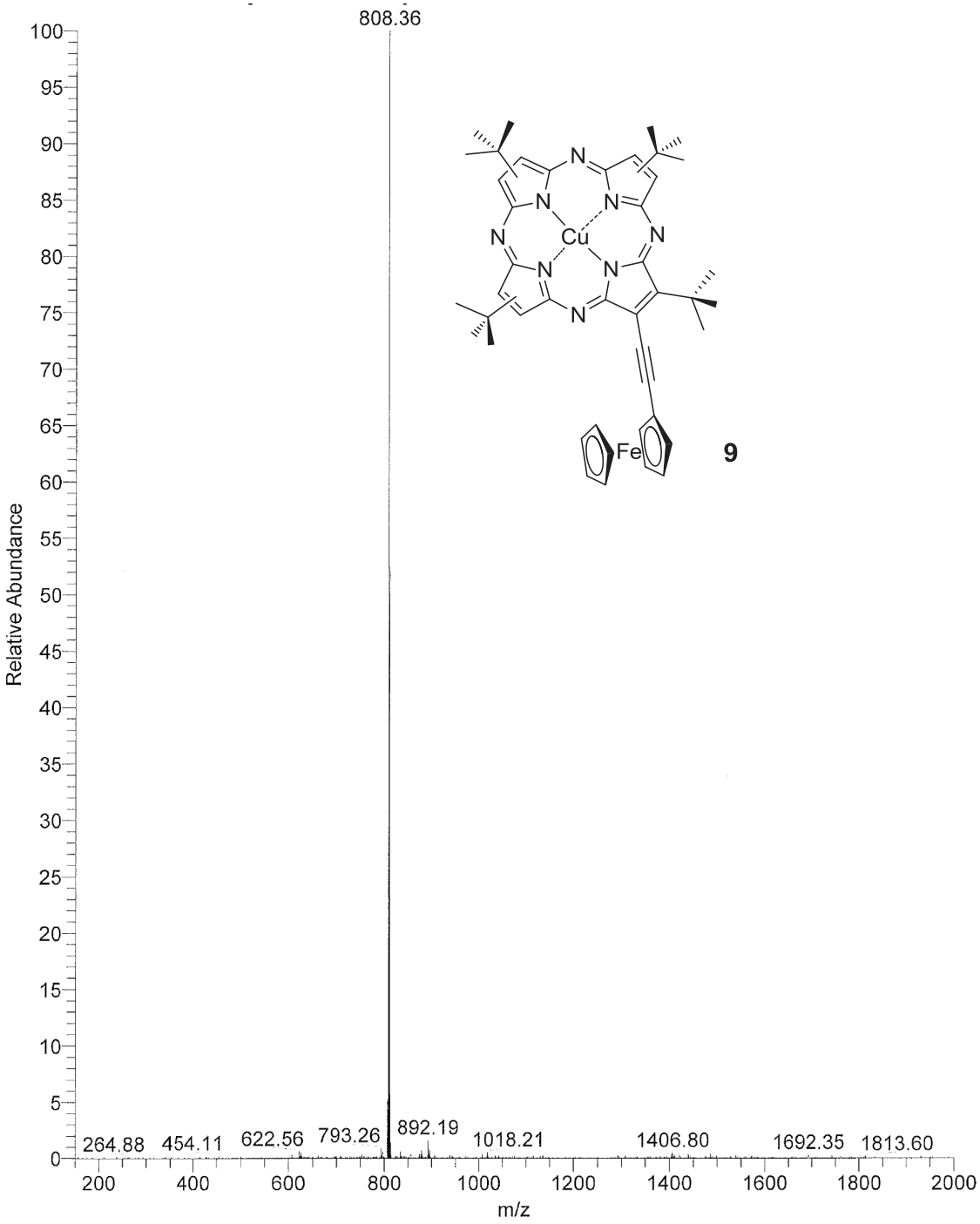

Figure 5. APCI MS spectrum of complex **9**.

classic e_g symmetry MO pair; these orbitals are well separated by energy from the LUMO+2. Similar to ferrocene-containing porphyrins, the electronic structure of **8Zn** and **9Zn** complexes predicts the possibility of a large number of predominantly metal-to-ligand charge transfer (MLCT) bands in the Q-band region, which could be heavily mixed into the tetraazaporphyrin-centered $\pi - \pi^*$ transitions. This can explain the broadening of the Q-band region observed in the UV-vis and MCD spectra of **8** and **9**.

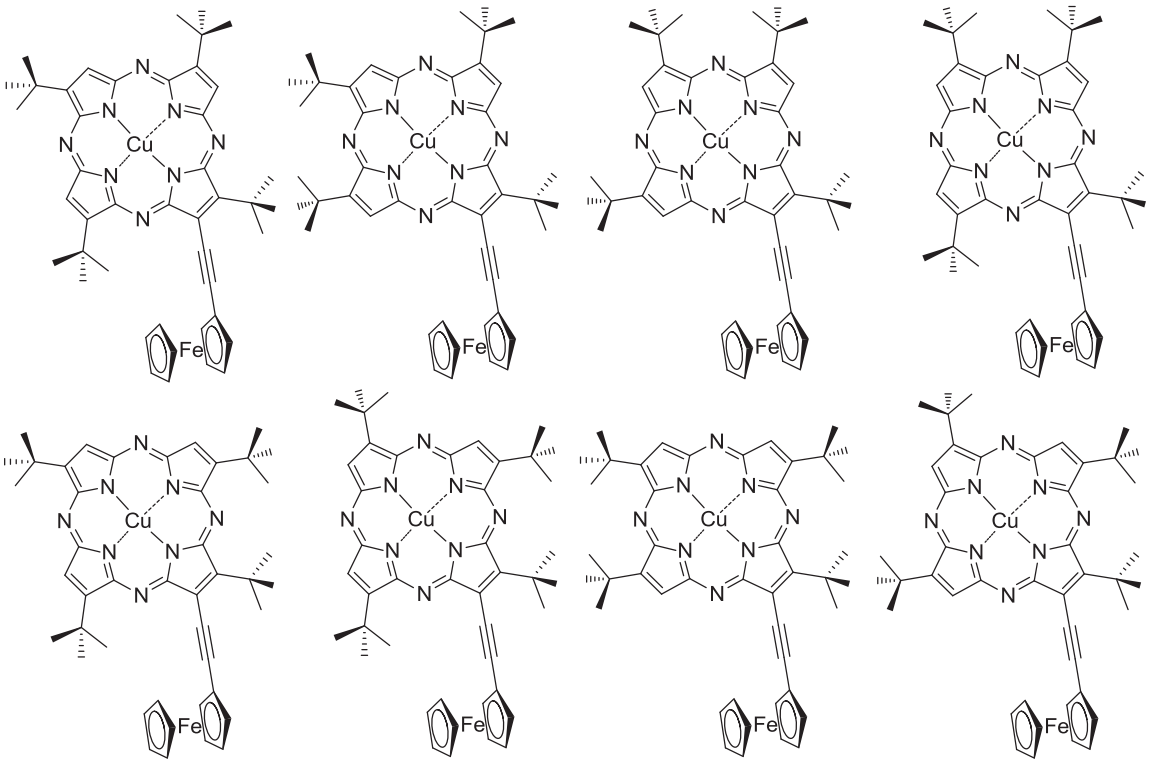

Figure 6. Positional isomers of complex **9**.

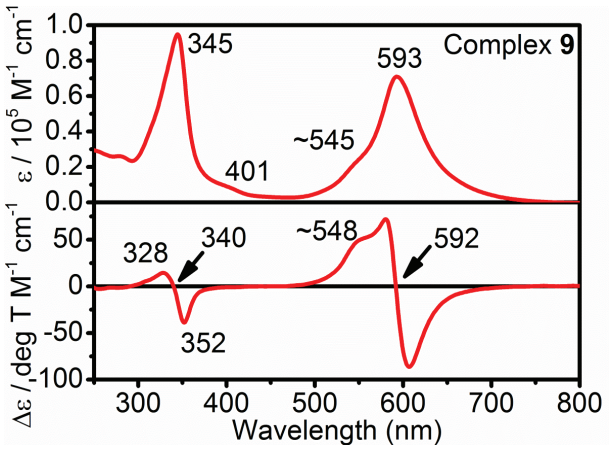

Figure 7. UV-vis (top) and MCD (bottom) spectra of complex **9** in DCM.

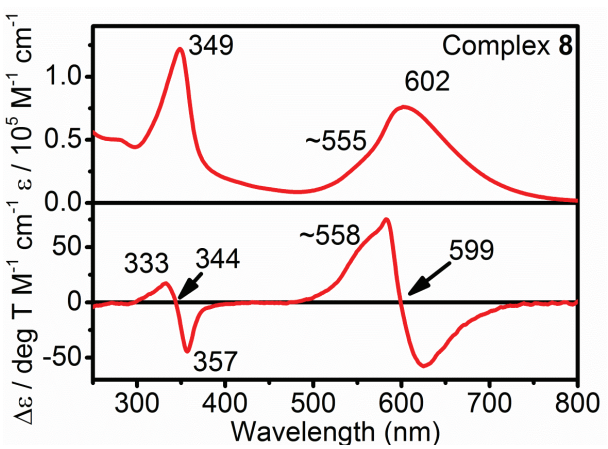

Figure 8. UV-vis (top) and MCD (bottom) spectra of complex **8** in DCM.

2.3. X-ray structures of 10 and 12

During TLC purification of the reaction mixtures originated from the Castro–Stephens coupling reaction[51] between di- and tetrabromo tetraazaporphyrins **1** and **2** and (ferrocenylethynyl)copper, we were able to crystallize individual isomers of copper mono- and tetrabromo tetraazaporphyrins **10** and **12** (Figure 15; Table). In the absence of ferrocene-substituents, these compounds have classic tetraazaporphyrin spectra with narrow Q- and

B-band regions, which consist of $\pi - \pi^*$ transitions (Figure 9). Crystal structures of **10** and **12** confirmed the formation of the proposed isomers and represent the first ever reported structures of a tetra-*tert*-butyl tetraazaporphyrin core. A common feature of structures **10** and **12** is the formation of dimers due to $\pi \cdots \pi$ stacking. Because of such interactions the tetraazaporphyrin core is lightly bent towards the 2 dimer molecules. The distance between the 2 aromatic planes is 3.255(12) Å and such dimers are packed in crystal by C-H$\cdots\pi$ and Br$\cdots\pi$ interactions perpendicular to each other. Copper centers are in square-planar geometry: Cu-N distances are 1.887(19)-1.959(18) Å and 1.914(10)-1.949(11) Å for **10** and **12**, respectively. All N–Cu–N angles are close to the normal 90° and 180°.

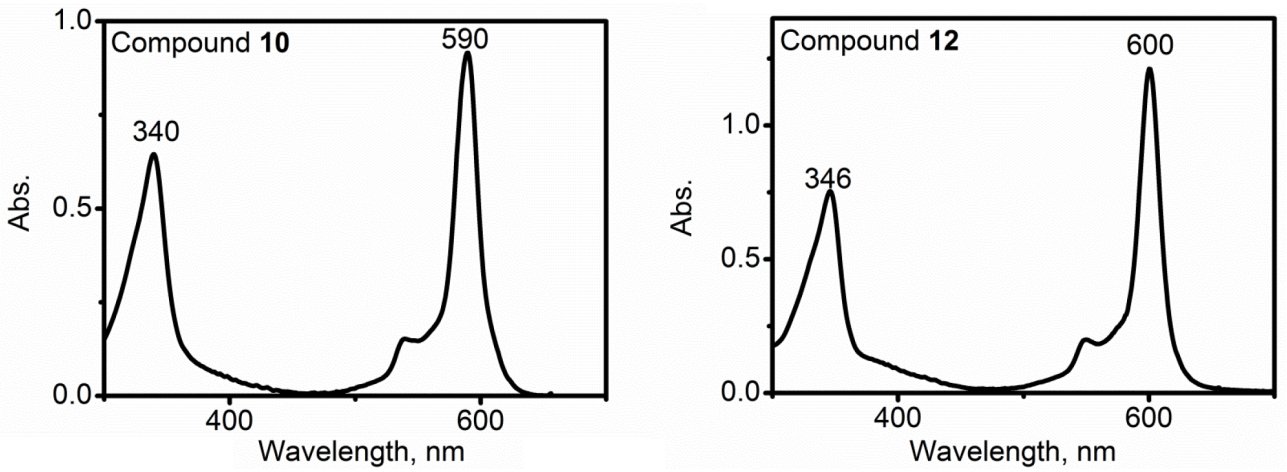

Figure 9. UV-vis spectra of complexes **10** (top) and **12** (bottom) in DCM.

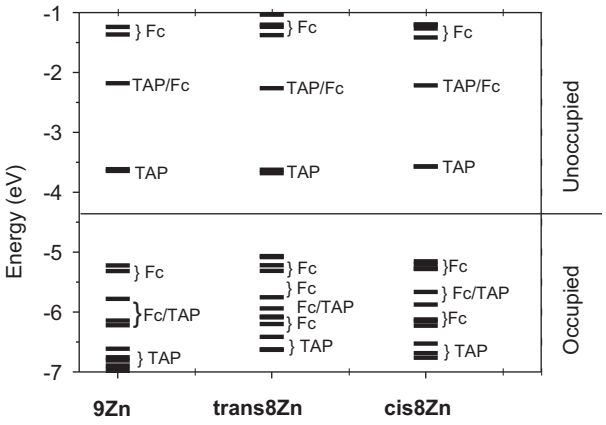

Figure 10. Energy diagram for complexes **trans8Zn**, **cis8Zn**, and **9Zn** calculated at DFT TPSSh/LANL2DZ level.

3. Conclusions

Two new mono- and bis-ferrocenylethynyl-containing copper tetraazaporphyrins were prepared under Castro–Stephens coupling reaction conditions starting from the metal-free 3(2),8(7)-dibromo- 2(3),7(8),12(13),17(18)-tetra-*tert*-butyl-5,10,15,20-tetraazaporphyrin and (ferrocenylethynyl)copper. Target complexes were purified as individual positional isomers, which were characterized by UV-vis, MCD, and APCI MS methods as well as DFT calculations. A similar reaction with metal-free 3(2),8(7),13(12),18(17)-tetrabromo-2(3),7(8),12(13),17(18)-

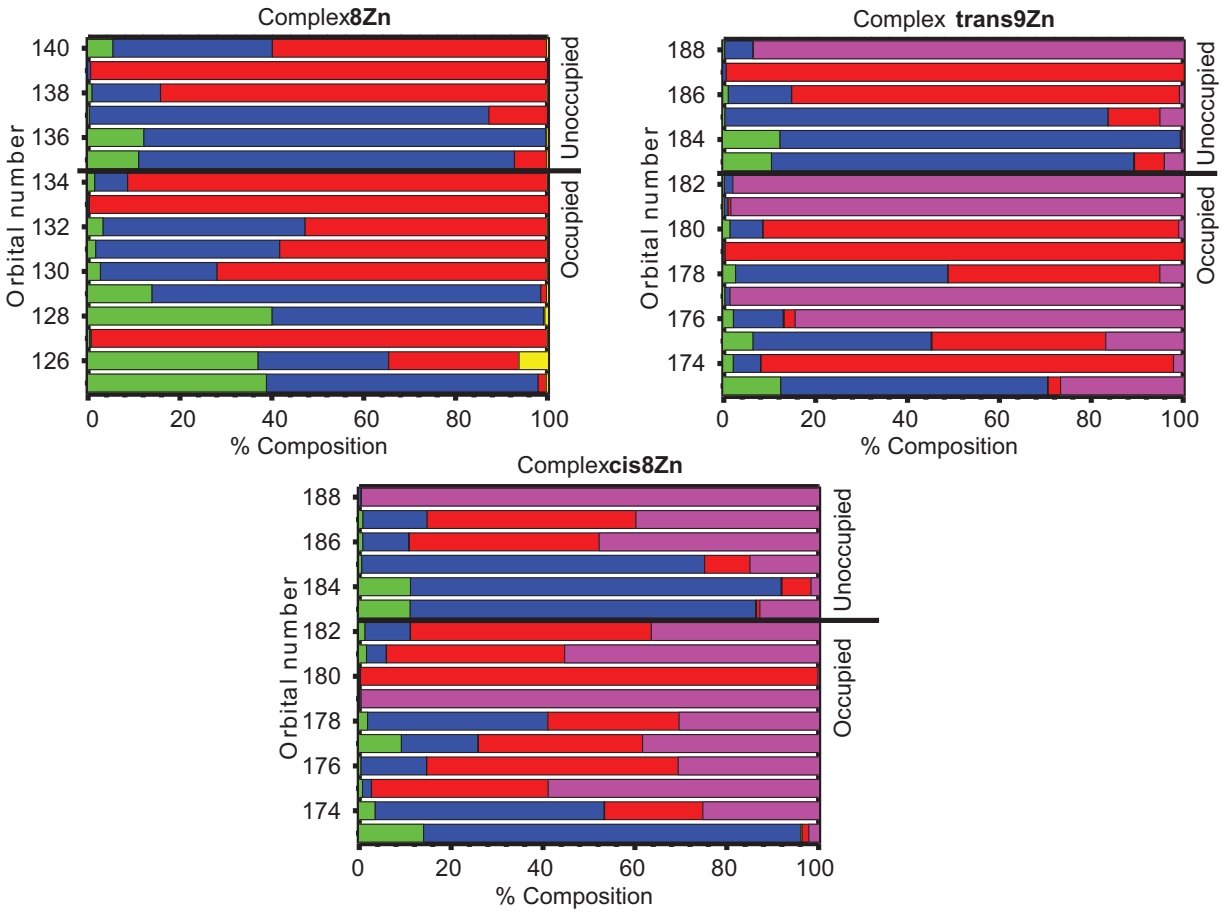

Figure 11. DFT orbitals composition for complexes **trans8Zn**, **cis8Zn**, and **9Zn** calculated at DFT TPSSh/LANL2DZ level.

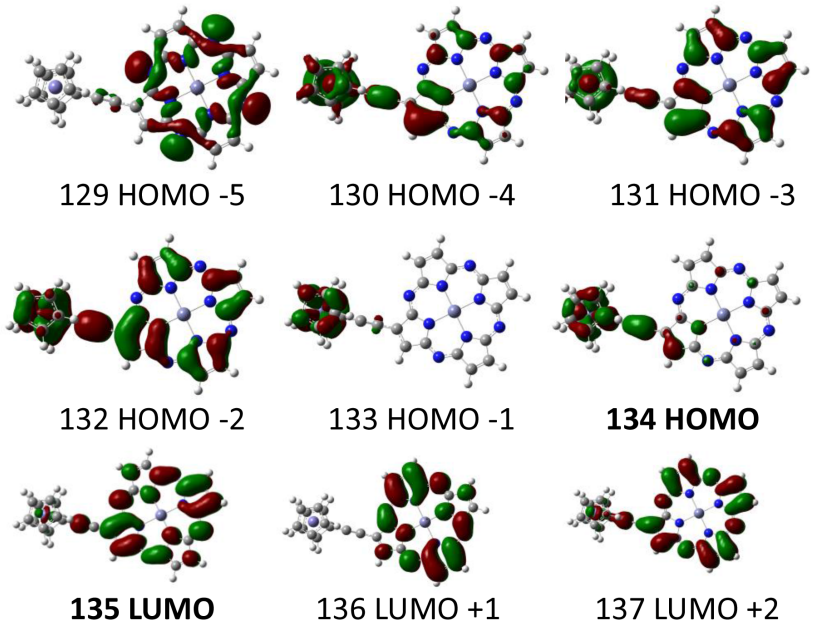

Figure 12. Plots of DFT orbitals for complex **9Zn** calculated at DFT TPSSh/LANL2DZ level.

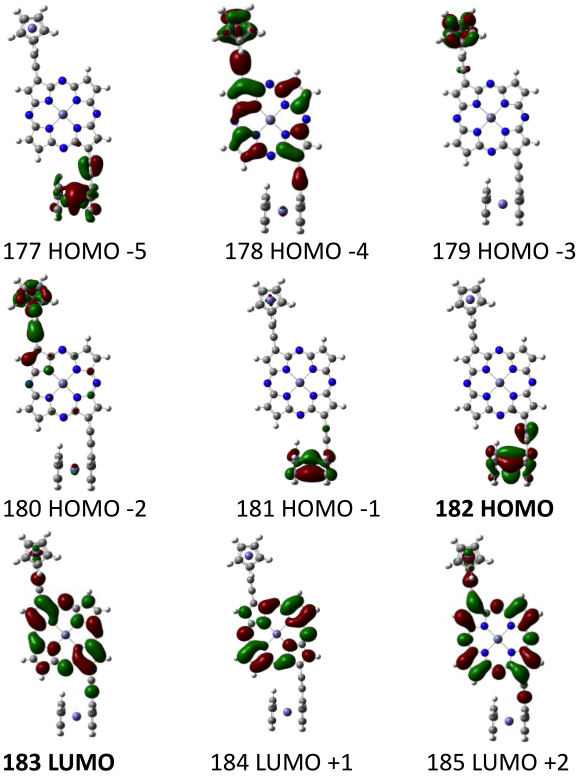

Figure 13. Plots of DFT orbitals for complex **trans8Zn** calculated at DFT TPSSh/LANL2DZ level.

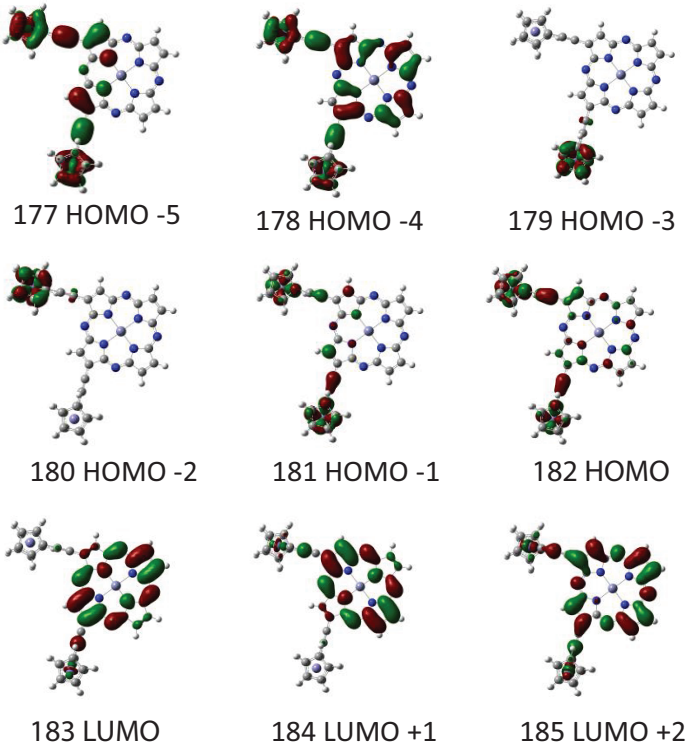

Figure 14. Plots of DFT orbitals for complex **cis8Zn** calculated at DFT TPSSh/LANL2DZ level.

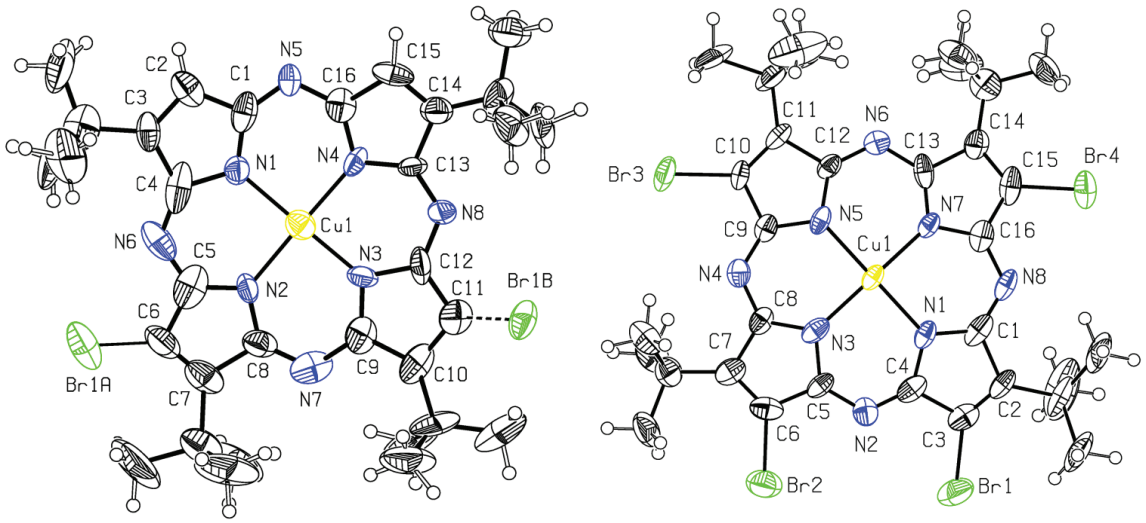

Figure 15. ORTEP diagram for the complex **10** (left) and complex **12** (right). Thermal ellipsoids are at 50% probability.

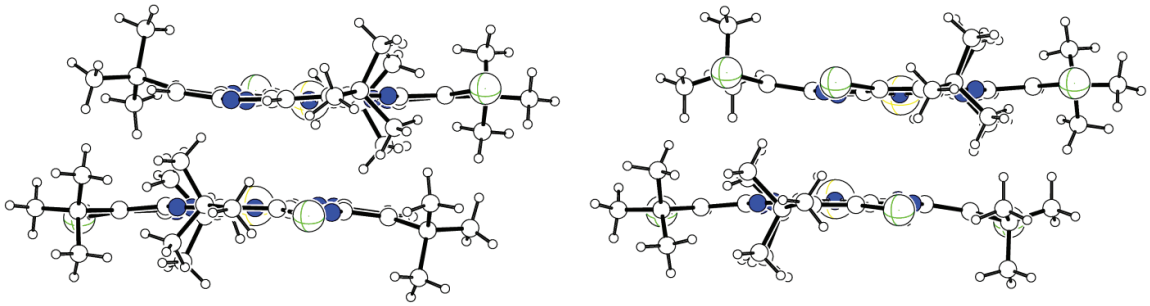

Figure 16. Packing diagram for the dimers of complex **10** (left) and complex **12** (right). Thermal ellipsoids are at 50% probability.

tetra-*tert*-butyl-5,10,15,20-tetraazaporphyrin resulted in the formation of only mono-ferrocenyl-containing complex. Direct coupling between ferrocene lithium and 3(2),8(7)-dibromo-2(3),7(8),12(13),17(18)-tetra-*tert*-butyl-5,10,15,20-tetraazaporphyrin resulted in a debromination reaction accompanied by minor tetraazaporphyrin dimerization, which was explained based on the steric properties of the parent tetraazaporphyrin. X-ray structures of individual positional isomers of copper 2-bromo-3,7,12,18-tetra-*tert*-butyl-5,10,15,20-tetraazaporphyrin and 3,7, 12,18-tetrabromo-2,8,13,17-tetra-*tert*-butyl-5,10,15,20-tetraazaporphyrin were also reported.

4. Experimental section

4.1. Materials

All reactions were performed under dry argon atmosphere with flame-dried glassware. All solvents and reagents were purchased from commercial sources and used without additional purification. Silica gel (60 Å, 63–100 μm) needed for column chromatography and TLC plates were purchased from Dynamic Adsorbents. SX-1 carrier for size-exclusion chromatography was purchased from Bio-Rad. 3(2),8(7)-Dibromo-2(3),7(8),12(13),17(18)-tetra-*tert*-butyl-5,10,15,20-tetraazaporphyrin (**1**) and 3(2),8(7),13(12),18(17)-tetrabromo-2(3),7(8),12(13),17(18)-tetra-*tert*-butyl-5,10,15,20-tetraazaporphyrin (**2**) were prepared using reported procedures.[49] (Ferrocenylethynyl)copper was prepared as described previously.[53]

Table. Crystal data collection and refinement for **10** and **12**.

	12	**10**
Empirical formula	$C_{32}H_{36}Br_4CuN_8$	$C_{32}H_{39}BrCuN_8$
Formula weight	915.87	679.16
Crystal system	Trigonal	Trigonal
Space group, Z	R-3: H, 18	R-3: H, 18
a (Å)	33.526(2)	33.755(8)
b (Å)	33.526(2)	33.755(8)
c (Å)	15.914(2)	14.812(7)
α (°)	90	90
β (°)	90	90
γ (°)	120	120
Volume (Å^3)	15,491(3)	14,616(10)
ρ_{calc}(g/cm^3)	1.767	1.389
μ(Mo–K$_\alpha$)(mm^{-1})	5.313	1.937
$\theta_{\max}$(°)	25.053	22.494
GoF(F^2)	1.064	0.925
R$_1^a$ (F^2 > 2σ(F^2))	0.0968	0.1103
wR$_2^b$ (all data)	0.2813	0.4069
$\Delta\rho_{\max}/\Delta\rho_{min}$ (e/Å^3)	3.116 / -1.262	1.044 / -0.483

^{a} $R_1(F) = \sum ||F_o| - |F_c|| / \sum |F_o|$. ^{b} $wR_2(F^2) = \{\sum [w(F_o^2 - F_c^2)^2] / \sum w(F_o^2)^2]\}^{1/2}$.

4.2. Computational aspects

All computations were performed using Gaussian 09 software running under Windows or UNIX OS.[54] Molecular orbital contributions were compiled from single point calculations using the QMForge program.[55] In all single-point calculations and geometry optimizations, a hybrid TPSSh (10% of Hartree–Fock exchange)[56] exchange correlation functional was used. The effective core potential LANL2DZ basis set[57] was used for all calculations.

4.3. X-ray crystallography

X-ray diffraction data were collected on an APEX-II CCD diffractometer using graphite-monochromated Mo-K$_\alpha$ radiation (λ = 0.71073 Å) at 123 K. Multiscan absorption corrections were applied to the data using the SAINT program.[58] The structures were solved by direct methods implemented in SHELXS-2013[59] and refined by full-matrix least squares based on F^2 using SHELXL-2013 and SHELXLE software. All nonhydrogen atoms were refined anisotropically, while hydrogen atoms were refined using "riding mode" with displacement parameters bonded to a parent atom: $U_{iso}(H) = 1.5U_{eq}(C)$ ($U_{eq} = 1/3(U_{11} + U_{22} + U_{33})$).

The tetraazaporphyrin molecule in the structure of complex **10** was found to be disordered. However, the disordered tetraazaporphyrin atoms from the components coincide and thus only the bromine atom was affected by the disorder. The occupancies were bonded to each other (total occupation is 1.0) and refined. Final occupation factors are 0.85 and 0.15. Some C–C bonds in –C(CH$_3$)$_3$ groups for both structures tend to be shorter. These bonds were restrained to the standard value 1.54(2) Å. Additionally, DELU/SIMU restrains were used for –C(CH$_3$)$_3$ groups.

4.4. Instrumentation

All UV-Vis data were obtained on a JASCO-720 spectrophotometer at room temperature. An OLIS DCM 17 CD spectropolarimeter with 1.4 T DeSa magnet was used to obtain all MCD data. APCI MS and MS/MS data were collected on an Agilent 1000 instrument using toluene/THF as a solvent.

4.5. Syntheses

4.5.1. Reaction between 3(2),8(7) -dibromo-2(3),7(8),12(13),17(18)-tetra-*tert*-butyl-5,10,15,20-tetraazaporphyrin (1) and (ferrocenylethynyl)copper

First 50 mg of 3(2),8(7)-dibromo-2(3),7(8),12(13),17(18)-tetra-*tert*-butyl-5,10,15,20-tetraazaporphyrin (0.07 mmol) and 80 mg of (ferrocenylethynyl)copper (0.28 mmol) were refluxed for 5 h in 10 mL of dry pyridine under argon atmosphere. The reaction mixture was then diluted with 30 mL of water, and dark precipitate was filtered, washed several times with water, and dried. The precipitate was dissolved in chloroform and filtered through a short silica gel plug to eliminate polar impurities. The collected blue fraction was further purified using a size exclusion SX-1 column with chloroform as eluent. Four colored fractions were collected, which were identified by mass spectrometry as complexes **8**–**11**. Each of these fractions was further purified using the TLC plates. Bisferrocenyl-containing complex **8** was separated into 2 individual positional isomers (**8a**, R_f = 0.24 and **8b**, R_f = 0.22, overall yield: ~1 mg, 1.4%) using hexane:toluene (2:3 v/v) as eluent. Monoferrocenyl-containing complex **9** was separated into 3 individual positional isomers (**9a**, R_f = 0.44, 7 mg, 12.1%; **9b**, R_f = 0.15, 2 mg, 3.4%; and **9c**, R_f = 0.09, 4 mg, 6.9%) using hexane:toluene (2:3 v/v) as eluent. Monobromo complex **10** was separated into 2 individual positional isomers (**10a**, R_f = 0.65, 15 mg, 26.6% and **10b**, R_f = 0.20, 7 mg, 14.3%) using hexane:toluene (2:3 v/v) as eluent. Suitable for X-ray crystallography, single crystals of **10a** were grown from its saturated solution in toluene:hexane (1:1 v/v). Copper tetrazaporphyrin **11** was purified using the TLC approach as a single fraction (12 mg, 27.9% yield).

4.5.2. Reaction between 3(2),8(7),13(12),18(17)-tetrabromo-2(3),7(8),12(13),17(18)-tetra-*tert*-butyl-5,10,15,20-tetraazaporphyrin (1) and (ferrocenylethynyl)copper

First, 43 mg of 3(2),8(7),13(12),18(17)-tetrabromo-2(3),7(8),12(13),17(18)-tetra-*tert*-butyl-5,10,15,20-tetraazaporphyrin (0.05 mmol) and 160 mg of (ferrocenylethynyl)copper (0.56 mmol) were refluxed for 5 h in 10 mL of dry pyridine under argon atmosphere. The reaction mixture was then diluted with 30 mL of water, and dark precipitate was filtered, washed several times with water, and dried. The precipitate was dissolved in chloroform and filtered through a short silica gel plug to eliminate polar impurities. The reaction mixture was analyzed using APCI mass spectrometry and revealed 2 major products: copper tetrabromo derivative **12** and monoferrocenyl-containing tribromo complex **13**. These were separated using a size exclusion SX-1 column with chloroform as eluent. Complex **12** was isolated in 35 mg (76%) yield. Suitable for X-ray crystallography, single crystals of this complex were grown from toluene solution. Monoferrocenyl-containing tribromo complex **13** was isolated only in trace quantities and was not characterized in detail.

4.5.3. Reaction between 3(2),8(7)-dibromo-2(3),7(8),12(13),17(18)-tetra-*tert*-butyl-5,10,15,20-tetraazaporphyrin (1) and ferrocenyl lithium

First 50 mg of 3(2),8(7)-dibromo-2(3),7(8),12(13),17(18)-tetra-*tert*-butyl-5,10,15,20-tetraazaporphyrin (0.07 mmol) and 54 mg of ferrocenyl lithium (0.28 mmol)[60] were refluxed for 5 h in 10 mL of dry THF under

argon atmosphere. The solvent was evaporated to dryness, and the dark blue precipitate was filtered, washed several times with water, and dried. The residue was dissolved in chloroform and filtered through a short silica gel plug to eliminate polar impurities. The reaction mixture was analyzed using APCI mass spectrometry and revealed only bromine elimination products along with a small amount of dimeric tetraazaporphyrins. Column chromatography on the reaction mixture (toluene:hexane 1:1 v/v) resulted in 3 blue fractions. The first fraction consists of dimer **3** along with its dibromo- monobromo- derivatives **5** and **4** (trace amounts, Scheme 1). The second and third fractions contain starting material along with monobromo derivative **6** and regular tetraazaporphyrin **7**. Since these compounds have no ferrocene substituents, no further attempt for their separation was made.

Acknowledgments

Generous support from the NSF CHE-1110455, CHE-1401375, and NSF MRI CHE-0922366, Minnesota Supercomputing Institute, and U of M Grant-in-Aid to VN is greatly appreciated.

References

1. Nemykin, V. N.; Lukyanets, E. A. *ARKIVOC*, **2010**, (i), 136–208.
2. Nemykin, V. N.; Lukyanets, E. A. In *Handbook of Porphyrin Science*, Vol. 3, Kadish, K. M.; Smith, K. M.; Guilard R. (Eds.); World Scientific: Singapore, 2010, pp 1–323.
3. McKeown, N. B. *Phthalocyanine Materials: Structure, Synthesis and Function*; Cambridge Univ. Press: Cambridge, UK, 1998.
4. Nemykin, V. N.; Dudkin, S. V.; Dumoulin, F.; Hirel, C.; Gurek, A. G.; Ahsen, V. *ARKIVOC* **2014**, (i), 142–204.
5. Lukyanets, E. A. *J. Porphyrins Phthalocyanines* **1999**, *3*, 424–432.
6. De Rosa, A.; Naviglio, D.; Di Luccia, A. *Curr. Cancer Therapy Rev.* **2011**, *7*, 234–247.
7. Sorokin, A. B. *Chem. Rev.* **2013**, *113*, 8152–8191.
8. Sorokin, A. B.; Kudrik, E. V.; Bouchu, D. *Chem. Commun.* **2008**, 2562–2564.
9. Geraskin, I. M.; Luedtke, M. W.; Neu, H. M.; Nemykin, V. N.; Zhdankin, V. V. *Tetr. Lett.* **2008**, *49*, 7410–7412.
10. Hurditch, R. *Adv. Colour Sci. Technology* **2001**, *4*, 33–40.
11. Chen, X.; Li, C.; Graetzel, M.; Kostecki, R.; Mao, S. S. *Chem. Soc. Rev.* **2012**, *41*, 7909–7937.
12. D'Souza, F.; Ito, O. *Chem. Soc. Rev.* **2012**, *41*, 86–96.
13. Harbeck, S.; Atilla, D.; Dulger, I.; Harbeck, M.; Gurek, A. G.; Ozturk, Z. Z.; Ahsen, V. *Sensors Actuators, B: Chemical* **2014**, *191*, 750–756.
14. Fabre, B. *Acc. Chem. Res.* **2010**, *43*, 1509–1578.
15. Stepnicka P. (Ed.). *Ferrocenes: Ligands, Materials and Biomolecules*; John Wiley & Sons, Ltd.: Chichester, UK, 2008.
16. Vecchi, A.; Galloni, P.; Floris, B.; Nemykin, V. N. *J. Porphyrins Phthalocyanines* **2013**, *17*, 165–196.
17. Bucher, C.; Devillers, C. H.; Moutet, J.-C.; Royal, G.; Saint-Aman, E. *Coord. Chem. Rev.* **2009**, *253*, 21–36.
18. Suijkerbuijk, B. M. J. M.; Klein Gebbink, R. J. M. *Angew. Chem., Int. Ed.* **2008**, *47*, 7396–7421.
19. Galloni, P.; Floris, B.; de Cola, L.; Cecchetto, E.; Williams, R. M. *J. Phys. Chem. C* **2007**, *111*, 1517–1523.
20. Lvova, L.; Galloni, P.; Floris, B.; Lundstroem, I.; Paolesse, R.; Di Natale, C. *Sensors* **2013**, *13*, 5841–5856.
21. Nemykin, V. N.; Rohde, G. T.; Barrett, C. D.; Hadt, R. G.; Bizzarri, C.; Galloni, P.; Floris, B.; Nowik, I.; Herber, R. H.; Marrani, A. G.; Zanoni, R.; Loim, N. M. *J. Am. Chem. Soc.* **2009**, *131*, 14969–14978.

22. Nemykin, V. N.; Barrett, C. D.; Hadt, R. G.; Subbotin, R. I.; Maximov, A. Y.; Polshin, E. V.; Koposov, A. Y. *Dalton Trans.* **2007**, 3378–3389.
23. Nemykin, V. N.; Galloni, P.; Floris, B.; Barrett, C. D.; Hadt, R. G.; Subbotin, R. I.; Marrani, A. G.; Zanoni, R.; Loim, N. M. *Dalton Trans.* **2008**, 4233–4246.
24. Nemykin, V. N.; Rohde, G. T.; Barrett, C. D.; Hadt, R. G.; Sabin, J. R.; Reina, G.; Galloni, P.; Floris, B. *Inorg. Chem.* **2010**, *49*, 7497–7509.
25. Rohde, G. T.; Sabin, J. R.; Barrett, C. D.; Nemykin, V. N. *New J. Chem.* **2011**, *35*, 1440–1448.
26. Dammer, S. J.; Solntsev, P. V.; Sabin, J. R.; Nemykin, V. N. *Inorg. Chem.* **2013**, *52*, 9496–9510.
27. Sirbu, D.; Turta, C.; Benniston, A. C.; Abou-Chahine, F.; Lemmetyinen, H.; Tkachenko, N. V.; Wood, C.; Gibson, E. *RSC Advances* **2014**, *4*, 22733–22742.
28. Su, M.; Li, Q.; Wang, Y.; Chen, S.; Zhao, H.; Bian, Z. *Chin. J. Org. Chem.* **2013**, *33*, 815–819.
29. Loim, N. M.; Abramova, N. V.; Sokolov, V. I. *Mendeleev Commun.* **1996**, 46–47.
30. Burrell, A. K.; Campbell, W. M.; Jameson G. B.; Officer, D. L.; Boyd, P. D. W.; Zhao, Z.; Cocks, P. A.; Gordon, K. C. *Chem. Commun.* **1999**, 637–638.
31. Narayanan, S.J.; Venkatraman, S.; Dey, S. R.; Sridevi, B.; Anand, V. R. G.; Chandrashekar, T. K. *Synlett* **2000**, 1834–1836.
32. Rhee, S. W.; Na, Y. H.; Do, Y.; Kim, J. *Inorg. Chim. Acta* **2000**, *309*, 49–56.
33. Shoji, O.; Okada, S.; Satake, A.; Kobuke Y. *J. Am. Chem. Soc.* **2005**, *127*, 2201–2210.
34. Shoji, O.; Tanaka, H.; Kawai, T.; Kobuke, Y. *J. Am. Chem. Soc.* **2005**, *127*, 8598–8599.
35. Rochford, J.; Rooney, A. D.; Pryce, M. T. *Inorg. Chem.* **2007**, *46*, 7247–7249.
36. Jin, Z.; Nolan, K.; McArthur, C. R.; Lever, A. B. P.; Leznoff, C. C. *J. Organomet. Chem.* **1994**, *468*, 205–212.
37. Poon, K.-W.; Yan, Y.; Li, X. Y.; Ng, D. K. P. *Organometallics* **1999**, *18*, 3528–3533.
38. Pomarico, G.; Vecchi, A.; Mandoj, F.; Bortolini, O.; Cicero, D. O.; Galloni, P.; Paolesse, R. *Chem. Commun.* **2014**, *50*, 4076–4078.
39. Gryko, D. T.; Piechowska, J.; Jaworski, J. S.; Galezowski, M.; Tasior, M.; Cembor, M.; Butenschoen, H. *New J. Chem.* **2007**, *31*, 1613–1619.
40. Ziegler, C. J.; Chanawanno, K.; Hasheminsasab, A.; Zatsikha, Y. V.; Maligaspe, E.; Nemykin, V. N. *Inorg. Chem.* **2014**, *53*, 4751–4755.
41. Misra, R.; Dhokale, B.; Jadhav, T.; Mobin, S. M. *Dalton Trans.* **2013**, *42*, 13658–13666.
42. Galangau, O.; Fabre-Francke, I.; Munteanu, S.; Dumas-Verdes, C.; Clavier, G.; Meallet-Renault, R.; Pansu, R. B.; Hartl, F.; Miomandre, F. *Electrochimica Acta* **2013**, *87*, 809–815.
43. Liu, J.-Y.; El-Khouly, M. E.; Fukuzumi, S.; Ng, D. K. P. *ChemPhysChem* **2012**, *13*, 2030–2036.
44. Bandi, V.; El-Khouly, M. E.; Ohkubo, K.; Nesterov, V. N.; Zandler, M. E.; Fukuzumi, S.; D'Souza, F. *J. Phys. Chem. C* **2014**, *118*, 2321–2332.
45. Nemykin, V. N.; Kobayashi, N. *Chem. Commun.* **2001**, 165–166.
46. Lukyanets, E. A.; Nemykin, V. N. *J. Porphyrins Phthalocyanines* **2010**, *14*, 1–40.
47. Nemykin, V. N.; Makarova, E. A.; Grosland, J. O.; Hadt, R. G.; Koposov, A. Y. *Inorg. Chem.* **2007**, *46*, 9591–9601.
48. Nemykin, V. N.; Maximov, A. Y.; Koposov, A. Y. *Organometallics* **2007**, *26*, 3138–3148.
49. Kopranenkov, V. N.; Makarova, E. A.; Shevtsov, V. K.; Lukyanets, E. A. *Khim. Geterotsikl. Soed.* **1994**, 1206–1212.
50. Fittig, R.; König, J. *Ann. Chem. Pharm.* **1867**, *144*, 277–294.
51. Stephens, R. D.; Castro, C. E. *J. Org. Chem.* **1963**, *28*, 3313–3315.
52. Gouterman, M. *J. Mol. Spectrosc.* **1961**, *6*, 138–163.

53. Bildstein, B.; Schweiger, M.; Kopacka, H.; Ongania, K.-H.; Wurst, K. *Organometallics* **1998**, *17*, 2414–2424.

54. *Gaussian 09, Revision A.1*, Frisch, M. J.; Trucks, G. W.; Schlegel, H. B.; Scuseria, G. E.; Robb, M. A.; Cheeseman, J. R.; Scalmani, G.; Barone, V.; Mennucci, B.; Petersson, G. A.; et al. Gaussian, Inc., Wallingford CT, **2009**.

55. QMForge program: http://qmforge.sourceforge.net/.

56. Tao, J.; Perdew, J. P.; Staroverov, V. N.; Scuseria, G. E. *Phys. Rev. Lett.* **2003**, *91*, 146401/1-146401/4.

57. Hay, P. J.; Wadt, W. R. *J. Chem. Phys.* **1985**, *82*, 270–283.

58. Sheldrick, G. M. *Acta Crystallogr.* **2008**, *A64*, 112.

59. Hübschle, C. B.; Sheldrick, G. M.; Dittrich B. *J. Appl. Cryst.* **2011**, *44*, 1281–1284.

60. Solntsev, P. V.; Sabin, J. R.; Dammer, S. J.; Gerasimchuk, N. N.; Nemykin, V. N. *Chem. Commun.* **2010**, *46*, 6581–6583.